

---

# QuickBind: A Light-Weight And Interpretable Molecular Docking Model

---

**Wojtek Treyde\***

Department of Systems Biology  
Columbia University  
New York, NY  
wojtek.treyde@sjc.ox.ac.uk

**Seohyun Chris Kim**

Department of Systems Biology  
Columbia University  
New York, NY

**Nazim Bouatta**

Department of Systems Biology  
Harvard Medical School  
Boston, MA

**Mohammed AlQuraishi**

Department of Systems Biology  
Columbia University  
New York, NY  
m.alquraishi@columbia.edu

## Abstract

Predicting a ligand's bound pose to a target protein is a key component of early-stage computational drug discovery. Recent developments in machine learning methods have focused on improving pose quality at the cost of model runtime. For high-throughput virtual screening applications, this exposes a capability gap that can be filled by moderately accurate but fast pose prediction. To this end, we developed QUICKBIND, a light-weight pose prediction algorithm. We assess QUICKBIND on widely used benchmarks and find that it provides an attractive trade-off between model accuracy and runtime. To facilitate virtual screening applications, we augment QUICKBIND with a binding affinity module and demonstrate its capabilities for multiple clinically-relevant drug targets. Finally, we investigate the mechanistic basis by which QUICKBIND makes predictions and find that it has learned key physicochemical properties of molecular docking, providing new insights into how machine learning models generate protein-ligand poses. By virtue of its simplicity, QUICKBIND can serve as both an effective virtual screening tool and a minimal test bed for exploring new model architectures and innovations. Model code and weights are available at this GitHub repository.

## 1 Introduction

Small organic molecules ("ligands") are a major class of drugs that act by binding protein targets, thereby affecting their functionality and interfering with the molecular pathways of diseases. Their distinct advantages, including ease of synthesis, administration, and cell permeability, render them indispensable as a pharmaceutical modality. In early-stage drug discovery, structure determination of protein-ligand complexes is a critical scientific tool, as it can provide an understanding of the molecular determinants of binding and enable further optimization of drug affinity and selectivity. It is however bottlenecked by costly and cumbersome experimental procedures, which computational "molecular docking" promises to overcome. When supplemented by an estimate of the strength of the binding interaction, computational tools can be used to virtually screen very large spaces of drug-like molecules [1] for viable drug candidates that can serve as starting hypotheses for subsequent experimental investigation and development [2, 3]. Existing

---

\*Present address: Department of Chemistry, University of Oxford, Oxford, UK.

computational methods achieve high-quality predictions at the cost of increasingly long runtimes, caused, in the case of conventional physical methods, by the need to sample numerous binding locations and poses, and in the case of machine learning (ML)-based methods by the complexity of the underlying neural computations that implicitly do the same.

Modern methods can be largely divided into molecular docking and co-folding. In molecular docking, an approximate protein structure is assumed to be known, whereas in co-folding both protein and ligand structures are predicted from scratch. Although a new development, co-folding has become the focus of much recent research activity, including ROSETTAFOLD ALL-ATOM (RFAA) [4], NEURALPLEXER [5], UMOL [6], and ALPHAFOLD 3 (AF3) [7]. Nonetheless, for drug discovery campaigns against a known and potentially well-studied protein target, it is often unnecessary to predict protein structures independently for every ligand, making molecular docking an attractive alternative given its higher speed (due to the assumed rigidity of the protein).

ML-based docking methods can be further divided into targeted docking, which requires specifying the approximate binding pocket, and blind docking, which does not. The first ML method to tackle the latter is EQUIBIND [8], which predicts the isolated, bound conformation of the ligand and uses a keypoint alignment mechanism to identify the rotation and translation needed to dock the ligand into the binding pocket. Subsequent methods employ more complex architectures. In particular, TANKBIND [9] and E3BIND [10] first partition the protein into functional blocks using P2Rank [11], predict the interaction of the given ligand with each block, and choose the final pose based on the predicted binding affinity (TANKBIND) or confidence score (E3BIND). Both architectures include components inspired by ALPHAFOLD 2’s (AF2’s) Evoformer module [12]. Importantly, TANKBIND predicts an intermolecular distance map that is converted into final coordinates by numerical post-optimization, whereas E3BIND operates on the ligand coordinates directly. FABIND [13] builds upon E3BIND by integrating the prediction of the location of the binding pocket into the main model, such that the whole process becomes end-to-end differentiable. Another leap forward was made by DIFFDOCK [14], a diffusion-based generative model that, starting from an input conformer, predicts changes in torsion angles as well as the transformation needed to dock the ligand into the protein. The inductive bias to focus only on relevant degrees of freedom coupled with a generative formulation led to large improvements in accuracy (and increased runtimes). More recently, advances have come from integration of protein language models [15], pretraining techniques geared towards molecular docking tasks, substantial increases in model size, and a shift towards generative approaches [14, 5, 7]. In combination, these trends have led to considerable increases in the computational cost of ML-based molecular docking, at levels prohibitive for virtual screening.

In this work we develop QUICKBIND, a light-weight method for rigid, blind molecular docking aimed at virtual screening applications by trading accuracy for speed. QUICKBIND performs well on the PDBBind test set, in particular when only unseen proteins are considered, and is substantially faster than DIFFDOCK. Leveraging the AF2 architecture and problem formulation (Figure 1), QUICKBIND reasons over proteins using a residue-level representation in lieu of an atomistic one, permitting fast but implicit accounting of side chain flexibility. To accommodate additional degrees of freedom introduced by small molecule ligands, QUICKBIND incorporates a new framing strategy for the Invariant Point Attention (IPA) module of AF2. We also include a binding affinity prediction module to facilitate virtual screen applications, a capability typically absent from docking and co-folding methods. We showcase the utility and versatility of QUICKBIND by predicting binding affinities and structures for multiple important drug targets across various protein families, and investigate the interpretability of our model to better understand the biophysical basis of its predictions.

## 2 Methods

### 2.1 Dataset and evaluation metrics

We train and test QUICKBIND using the PDBBind [17] dataset and additionally assess it using the PoseBusters (PB) Benchmark [18]. PDBBind has been widely used to assess molecular docking methods using a temporal split proposed by EQUIBIND [8]. It contains crystal structures and binding affinities for  $\sim 20,000$  protein-ligand complexes; the training and validation sets comprise 16,379 and 968 complexes, respectively, both published before 2019, while the test set contains 363 complexes published in 2019 or later. There is no

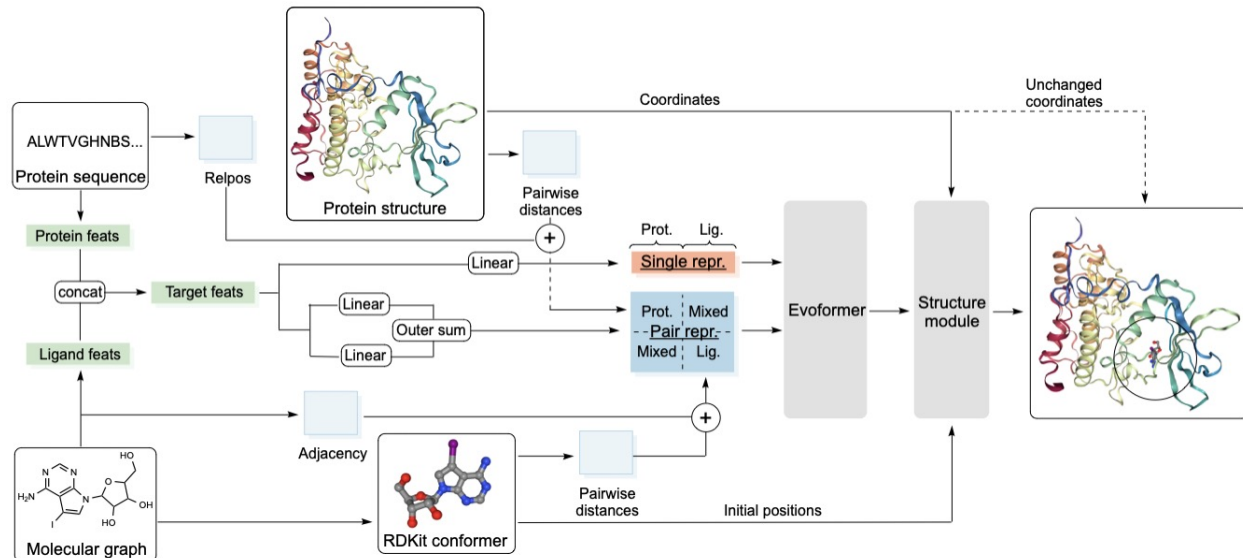


Figure 1: QUICKBIND architecture. A "single" representation is first constructed by concatenating embedded protein and ligand input features. A "pair" representation is then constructed from linear embeddings of the single representation, pairwise distances (of protein residues and ligands atoms, independently), relative positional encodings of protein residues, and the adjacency matrix of ligand atoms. The pair representation contains a protein and a ligand block, as well as mixed off-diagonal elements. The single and the pair representations are passed through a modified Evoformer stack, before the Structure module uses the updated single and pair representations as well as initial coordinates from an RDKit conformer [16] and protein coordinates from the input protein structure to dock the ligand into the binding pocket.

ligand overlap between the three partitions. PB contains 428 diverse complexes of unique proteins and drug-like ligands released since 2021, and is therefore disjoint from complexes in the PDBBind training set.

We quantify success based on the percentage of predictions with a symmetry-corrected ligand heavy atom root-mean-squared deviation (RMSD) of less than  $2\text{\AA}$  ("success rate"; [19, 20, 21, 22]). This criterion is widely used, as the residual deviation from the true bound conformation should not materially impact downstream analyses and optimizations. Evaluating models purely on success rate does not account for chemical and physical validity, but we assess these criteria using the PB suite [18]. Predictions that pass all PB tests and whose RMSD is below  $2\text{\AA}$  are deemed PB-valid.

## 2.2 Model architecture

QUICKBIND adapts the ALPHAFOLD 2 [12] architecture to the task of protein-ligand pose prediction (Figure 1). It takes as input protein sequence and structure as well as the chemical graph of the ligand and its 3D conformer (generated by the RDKit [16]). Inputs are combined to yield a unified first-order ("single") representation and a second-order pairwise ("pair") representation. These are then passed to a modified Evoformer stack that omits column-wise self-attention as multiple sequence alignments are not used. After processing by the Evoformer, a Structure module takes the updated single and pair representations as input as well as residue and ligand reference frames (using a new framing strategy for ligand atoms described below) and iteratively updates the ligand heavy atom coordinates. The Structure module is modified from AF2 so that the IPA module is gated [23], cross attention is performed between the single representations of the ligand and protein during the coordinate update step (Algorithm 3), and protein atoms are held fixed. QUICKBIND uses 12 Evoformer and 8 Structure module blocks. Full algorithm details are given in section SI.1.

AF2 uses reference frames to represent the geometry of protein residues: a translation vector corresponds to the coordinates of the  $C_{\alpha}$  atom while a rotation matrix, anchored at these coordinates, is canonically constructed from the N,  $C_{\alpha}$ , and C coordinates to encode the orientation of the residue backbone. This representation is natural for linear or branched polymers but for atoms of arbitrary small molecules, there are

no canonical frame construction approaches. With the emergence of co-folding methods, two recent models have proposed framing strategies for small molecules [4, 5], and QUICKBIND employs its own new approach. First, atom indices are reordered based on the canonical atom ranking of the RDKit [16]. For each heavy atom, its coordinates are treated as the  $C_\alpha$  atom and the coordinates of its two adjacent atoms with the lowest indices are treated as the N and C atoms. If an atom has only one bond, we use a dummy atom (Algorithm 4). We then construct atom reference frames using the same procedure employed for residue frames.

Using the above framing strategy, we found that during the IPA component of the Structure module, updating the rotation matrices of ligand atom frames improves performance, unlike the approaches of NEURALPLEXER and RFAA which only update the translation component and passively reconstruct the frames. We note that while AF3 does not use reference frames to reason over protein-ligand complexes, it does use a framing strategy to calculate the predicted aligned error. AF3’s reference frames are constructed using the two closest atoms to a given center atom, and when an atom does not have two neighbors, the frame is ignored. We experimented with an analogous strategy but found that our approach works better.

For the loss function we adopt a modified version of the frame-aligned point error (FAPE) used by AF2. FAPE is computed by performing a set of alignments such that the predicted reference frame of each residue is aligned with its original reference frame in the target structure. FAPE is then the average, clamped RMSD between the predicted and target structures over all alignments. For molecular docking, FAPE can be reformulated as a combination of two components: the RMSD between predicted and target ligand atom positions based on ligand frame alignments and residue frame alignments. The final QUICKBIND model was trained using this combined FAPE loss, intermediate FAPE losses acting on the outputs of every Structure module block, and a Kabsch RMSD loss corresponding to the ligand RMSD after superimposition of the predicted and target ligand using the Kabsch algorithm [24].

Further model details are given in sections SI.2-SI.5. Before training the final QUICKBIND model, aspects of the architecture were optimized using two smaller variants, QUICKBIND-S and QUICKBIND-M (section SI.4). The results of this hyperparameter screen are summarized in Table SI.1.

## 3 Results

### 3.1 Model performance

We first assess QUICKBIND on the PDBBind test set (Figure 2) and compare it to other ML-based rigid docking methods including EQUIBIND, TANKBIND, E3BIND, FABIND, DIFFDOCK, and NEURALPLEXER (employed for blind molecular docking rather than co-folding). We exclude co-folding methods from this comparison as they have not been evaluated on PDBBind. For virtual screening—which can involve billions of molecules [25]—docking runtimes are a critical consideration. With an average runtime of 2.7s, QUICKBIND is orders of magnitude faster than traditional docking methods [8], DIFFDOCK, and recent co-folding methods [4, 6, 7]. Accuracy-wise, QUICKBIND is middle-of-the-pack, outperforming most ML-based rigid docking methods except for FABIND, DIFFDOCK, and NEURALPLEXER, particularly when generalizing to proteins excluded from the training set. Excepting FABIND, these methods are all considerably slower, and FABIND still uses an order of magnitude more parameters.

Next, we assess QUICKBIND on the more challenging PB Benchmark (Figure 3) and include in our comparisons recent co-folding methods. QUICKBIND generally outperforms rigid docking methods (except DIFFDOCK but including FABIND) but trails co-folding methods. However, the speed gap between QUICKBIND and co-folding methods (which take minutes for a single prediction) is even more considerable, making QUICKBIND a compelling compromise between speed and accuracy. Figure SI.1 shows examples of highly accurate QUICKBIND predictions.

QUICKBIND forgoes a post-processing step common to most ML-based methods that enhance the chemical validity of predictions. As a result, QUICKBIND’s raw predictions do not generally pass the PB chemical and physical plausibility tests, largely due to incorrect bond lengths and angles (Figure SI.2, see also Figure SI.1a). As was noted in [18] however, such failures can typically be addressed by running a force field-based energy minimization post-prediction. Doing so does substantially improve the physical validity of QUICKBIND’s predictions and even slightly improves its success rate (Figure 3).

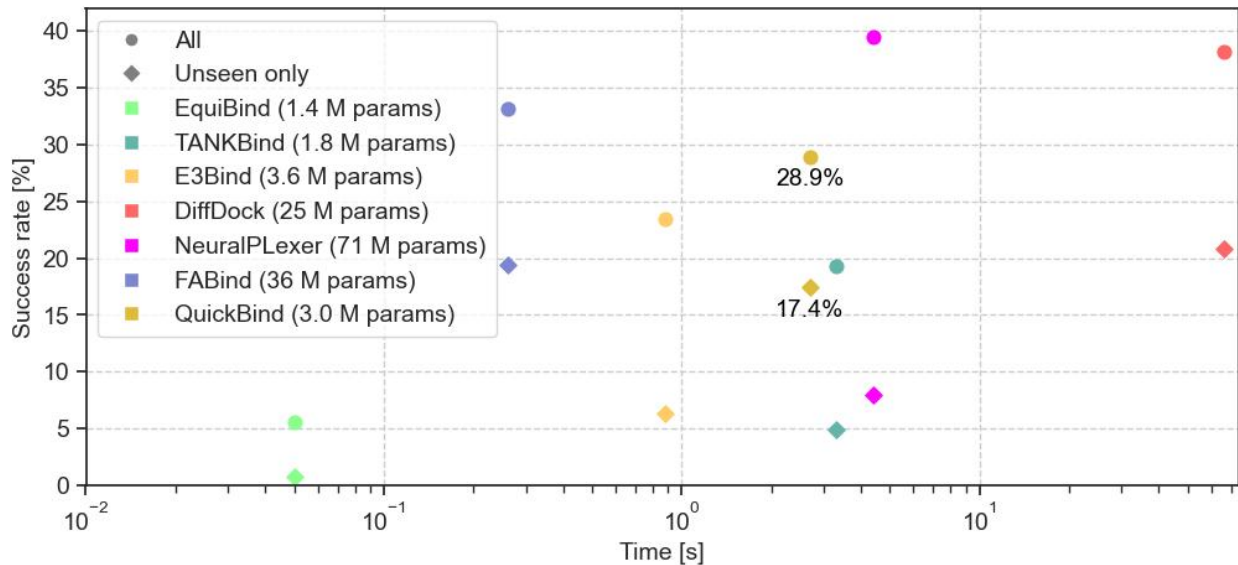


Figure 2: Success rates vs. average runtimes (summed over all complexes) for ML-based rigid docking methods on the PDBBind test set. Success rates are reported separately for all 363 complexes (circles) and for 144 complexes whose proteins are absent from the training and validation sets (diamonds). TANKBIND was only evaluated on a subset of 142 unseen proteins by its original authors. Success rates are taken from original publications, except for NEURALPLEXER’s success rate on unseen proteins as it was not originally reported. Runtimes do not include preprocessing and were determined on NVIDIA A40 GPUs using scripts provided in each method’s respective repository, without batching. NEURALPLEXER runtime excludes acquisition of auxiliary inputs (*e.g.*, AF2 predictions) while TANKBIND and E3BIND runtimes do not include P2Rank segmentation. E3BIND’s runtime was taken from its original publication since authors did not release the model weights and inference code.

Given its speed, a natural use case for QUICKBIND is binding affinity prediction for virtual screening applications. To test this potential, we trained a simple neural network to use QUICKBIND’s single representations (Algorithm 5) to predict protein-ligand affinities. We used the same PDBBind split as for training QUICKBIND and PDBBind’s own affinity data. The resulting model is competitive with other affinity predictors (Table SI.3) despite not having been optimized architecturally or through hyperparameter tuning. This indicates that QUICKBIND has immediate utility for virtual screening and may be further improved using more advanced top models for affinity prediction.

### 3.2 Model interpretability

Having trained QUICKBIND, we set out to investigate whether it had learned ligand characteristics relevant for molecular docking. Beyond binding affinity, molecular features such as lipophilicity and cell permeability can influence the outcome of drug discovery programs. These features are strongly linked to the physicochemical properties of ligands, such as hydrophobic surface area and molecular weight, to the extent that expert rules for drug design often explicitly restrict drug-like molecules based on these properties. A model that implicitly encodes them may thus hold promise for drug design beyond accurate pose prediction.

To this end, we extracted the single ligand representation from the Evoformer and transformed it into a molecule-level representation by averaging across atoms (Figure 4; pipeline schematic). For every resulting channel value, we computed Pearson’s R value for total hydrophobic surface area, molecular weight, number of hydrogen bond acceptors and donors, polar surface area, number of rotatable bonds, octanol-water partition coefficient, and number of aromatic rings; calculations were performed using the RDKit [16] and Mordred [26]. We carried out this computation for every molecule in the PDBBind test set (Figure 4; scatter plots). We found that some channels were significantly correlated with more than one property (Table SI.2,  $p$ -values were at least  $10^{-40}$ ; we did not correct for multiple hypothesis testing as there were only 64 channels),

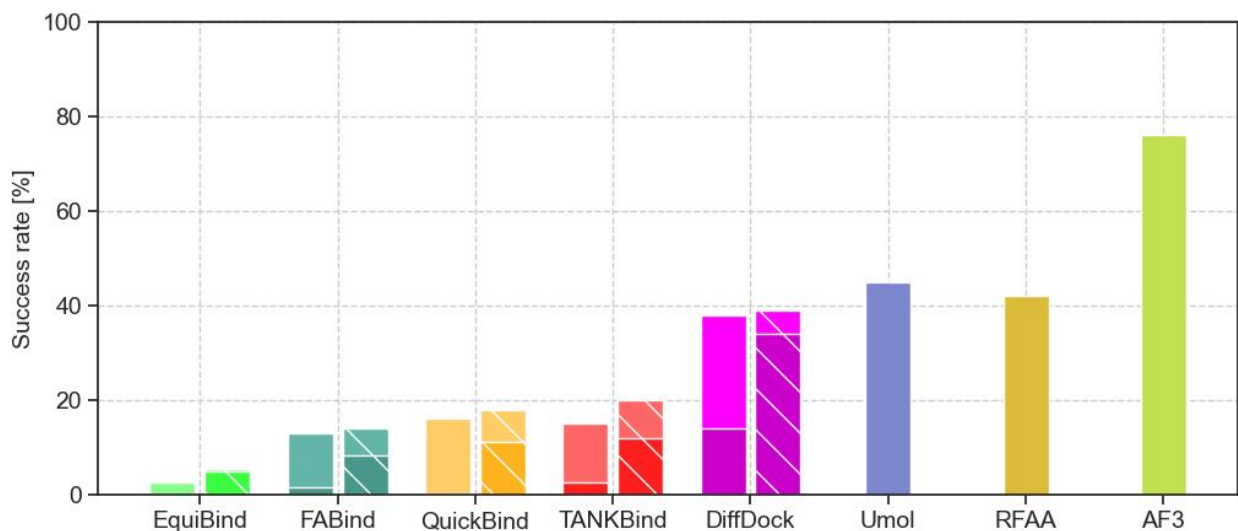


Figure 3: Success rates of ML-based rigid docking and co-folding models on the PB Benchmark, sorted in ascending order by model runtime (left-to-right). Target 7M31 was omitted for QUICKBIND because it is longer than 2,000 residues. Lighter colors correspond to all predictions while darker colors correspond to PB-valid predictions (docking methods only) and hatched bars to results after energy minimization. Success rates are taken from original publications [4, 6, 7, 18], except for FABIND’s success rate as it was not originally reported. We found the EQUIBIND success rates to be 0.9% (all predictions), 0.2% (PB-valid predictions), 4.2% (all predictions after energy minimization), and 3.5% (PB-valid predictions after energy minimization), in rough agreement with the originally reported values (2.6%, 0.0%, 5.5%, and 4.8%, respectively).

indicating that QUICKBIND has in fact learned physicochemical characteristics of protein-ligand binding. Selecting the most strongly correlated property per channel, we found the number of H-bond acceptors and donors, the total hydrophobic surface area, and the number of rotatable bonds to be the strongest features. We include additional results in section SI.9.

### 3.3 Case studies

To better understand QUICKBIND’s utility in real-world deployments, we predicted the bound poses of new ligands for five proteins in the PDBBind test set, which we selected based on their extensive experimental characterization and clinical significance (UniProt IDs B1MDI3, P56817, P17931, Q8ULI9, and P01116, Table SI.4). B1MDI3 is a tRNA guanine-methyltransferase, P56817 is BACE1, a beta-secretase relevant to the development of Alzheimer’s disease [27], P17931 is galectin-3, a galactose-specific lectin involved in cancer [28], Q8ULI9 is the human immunodeficiency virus 1 (HIV-1) protease, and P01116 is the GTPase K-Ras, a key cancer target. We used the protein crystal structures of the three lowest affinity binders from the PDBBind test set as input, and predicted the binding affinities and complex structures of all other compounds in the PDBBind test set. We treated all compounds not explicitly crystallized with the five target proteins as decoys (Figures SI.4-SI.6, Table SI.4). This likely resulted in some binders being mislabeled as non-binders.

We found QUICKBIND capable of discerning ligand binding characteristics across diverse ligand scaffolds and protein targets. Specifically, QUICKBIND distinguished binders from non-binders across various targets, including BACE1 ( $p$ -values of one-sided Wilcoxon rank sum tests of 0.0483, 0.0196, 0.0229), galectin-3 (0.0333, 0.0383, 0.0167), and K-Ras ( $< 0.00005$ , 0.0001, 0.0105), despite BACE1 and K-Ras binders having low average Tanimoto similarity. For BACE1 and galectin-3, QUICKBIND also accurately predicted poses with a ligand RMSD consistently below 2Å for the majority of ligands (success rates of 73% and 86%, respectively), based on our comparisons with PDBBind test set structures. For the HIV-1 protease, while the predicted binding affinities did not significantly differentiate binders from non-binders, QUICKBIND still excelled at predicting pose structures with high accuracy (all predictions below 2Å, Figure SI.7).



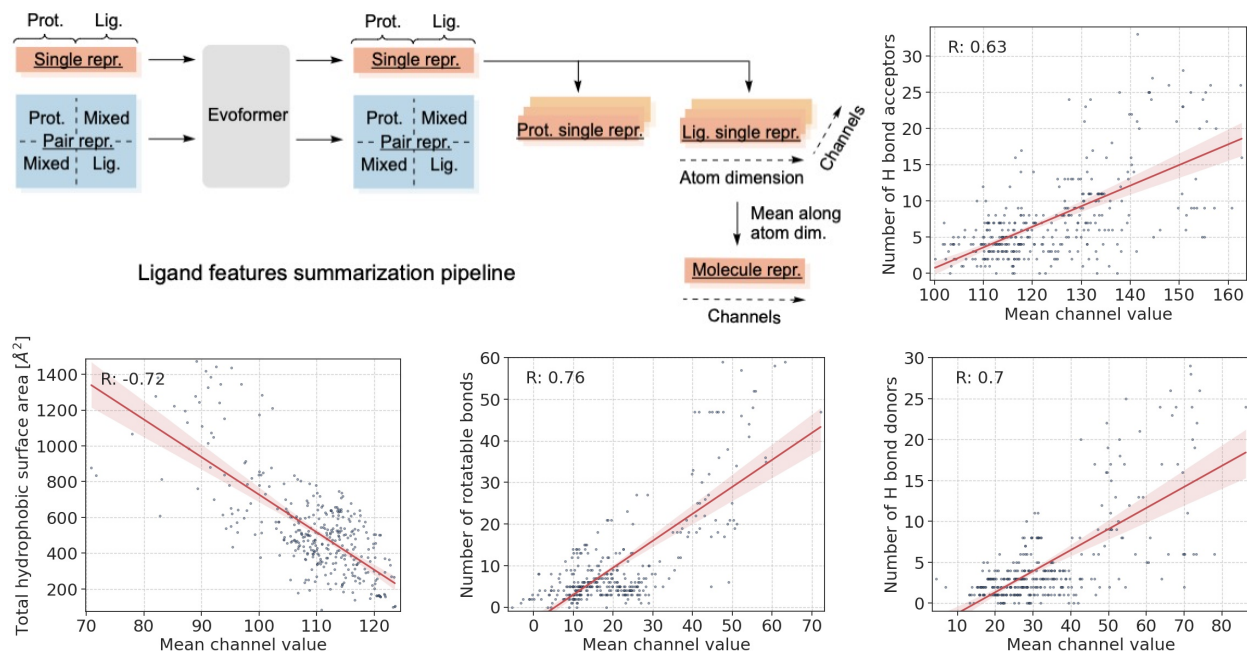


Figure 4: Interpretable physicochemical properties in QUICKBIND’s ligand representation. Processing the Evoformer’s single representation into separate protein and ligand representations followed by averaging the ligand’s atom dimension yields interpretable descriptors that correlate with channel values, including number of H-bond acceptors and donors, total hydrophobic surface area, and number of rotatable bonds.

Our analyses also shed light on the limitations of QUICKBIND. It struggled when confronted with proteins whose conformation changes dramatically when binding target ligands versus low affinity ligands used as templates. For instance, KRAS structures had an average backbone RMSD of 7.7Å between input and true conformations, which resulted in a notable proportion of poses exhibiting high ligand RMSDs (only 17% of predictions fell below 5Å). For the wholly unseen tRNA guanine-methyltransferase, QUICKBIND struggled to predict significantly higher binding affinities for binders vs. non-binders and only predicted moderately accurate poses with a ligand RMSD below 5Å in 2% of cases.

## 4 Discussion

QUICKBIND is an ML model for blind molecular docking that optimizes runtime speed while retaining competitive pose prediction accuracy, providing a compelling option for high-throughput virtual screening. It furthermore captures physicochemical ligand properties known to influence molecular docking. Interpretability informs what aspects of the underlying physics a model has captured and may, if sufficiently well-developed, help guide the design of drug compounds. These considerations are important given the large costs involved in identifying and prioritizing compounds for experimental testing and optimization.

Our augmentation of QUICKBIND with affinity prediction capabilities make it suitable for identifying new ligands, which we showcase using multiple highly relevant drug targets. Except for TANKBIND, existing blind docking and co-folding models do not predict binding affinities, and are therefore not applicable for screening applications. The combination of ligand pose and interaction strength can help in optimizing the potency and selectivity of drug candidates, although it remains to be seen how sensitive QUICKBIND is to minor structural changes, which can have profound effects on binding (so-called activity cliffs).

An added advantage of QUICKBIND’s formulation of binding affinity prediction is its lack of reliance on an experimental co-complex structure (unlike TANKBIND), due to having been trained separately from the main docking model. Embeddings from any protein-ligand pair can be used, whether the structure is predicted or experimentally-derived. This means that QUICKBIND’s affinity module can be trained on BindingDB [29],

a binding affinities database comprising millions of protein-ligand pairs, orders of magnitude more than structural complexes. Users can also rapidly finetune a binding affinity model for their own target proteins.

Evaluation using the PB Benchmark showed that QUICKBIND struggles to generate physically and chemically valid poses, but that many can be recovered by force field-based energy minimization. While energy minimization can increase model runtime, the binding affinity module can be used to first select a subset of promising compounds, whose poses can then be energy minimized.

## 5 Outlook

A major shortcoming of QUICKBIND and other ML-based molecular docking methods is their dependence on rigid re-docking, a task on which they are both trained and evaluated. In rigid re-docking, methods are provided with the *holo* protein structure that was originally co-crystallized with the query ligand, and the protein structure is not predicted. This does not reflect many real-world uses of molecular docking in which users only have access to the *apo* (unbound) structure or a *holo* structure co-crystallized with another ligand. Although QUICKBIND showed promise at cross-docking in the case studies we conducted, it did so only as long as the input protein did not deviate too much from the true structure. Ideally, models should be trained and evaluated in a flexible cross-docking setting, and in fact ML-based blind, flexible docking methods [30] have recently emerged. Future versions of QUICKBIND can be adapted into a flexible docking method capable of using *apo*, *holo*, or even predicted protein structures as input by updating protein residue frames as well as ligand frames. Alternatively, side chains can be made flexible by updating the rotational component of residue frames and side chain torsion angles.

Conceptually, one of our goals for QUICKBIND was to investigate how the AF2 architecture may be adapted to the task of docking and co-folding. While other docking [9, 10] and co-folding methods [4, 5, 6, 31] previously demonstrated that ideas and components from AF2 can be used in protein-ligand pose prediction, QUICKBIND uses essentially the entirety of AF2. This has provided multiple insights. First, it suggests that QUICKBIND could further benefit from AF2’s native confidence estimates and recycling, which were found to be important for AF2’s success. QUICKBIND could also benefit from more complicated, AF2-inspired loss functions, for example the structural violation loss which would likely lead to more PB-valid predictions. Second, QUICKBIND provides a rough estimate of how well an AF2-like model can perform molecular docking. The fact that it does not achieve state-of-the-art performance suggests that certain aspects of AF2 are not ideally suited for this task and anticipates some of the changes introduced in AF3, including a minimized MSA module and atomistic reasoning over ligands. Including further innovations from AF3 will likely result in an improved molecular docking tool (section SI.12). In turn, our findings also have implications for AF3. For instance, since QUICKBIND’s single representation captures physicochemical features of the ligand, it is likely that AF3’s single representation is highly information-dense as well, and may therefore be useful for tasks beyond pose prediction.

## Acknowledgments and Disclosure of Funding

We would like to thank Psivant Therapeutics for providing computational resources. W.T. acknowledges financial support from the Max Planck School Matter to Life. S.C.K. is supported by NIH grant R35GM150546.



## References

- [1] Kirkpatrick, P. & Ellis, C. Chemical space. *Nature* **432**, 823 (2004).
- [2] Ferreira, L. G., Dos Santos, R. N., Oliva, G. & Andricopulo, A. D. Molecular docking and structure-based drug design strategies. *Molecules* **20**, 13384–13421 (2015).
- [3] Lyu, J. *et al.* Ultra-large library docking for discovering new chemotypes. *Nature* **566**, 224–229 (2019).
- [4] Krishna, R. *et al.* Generalized biomolecular modeling and design with rosettafold all-atom. *Science* **384**, ead12528 (2024).
- [5] Qiao, Z., Nie, W., Vahdat, A., Miller, T. F. & Anandkumar, A. State-specific protein–ligand complex structure prediction with a multiscale deep generative model. *Nature Machine Intelligence* **6**, 195–208 (2024).
- [6] Bryant, P., Kelkar, A., Guljas, A., Clementi, C. & Noé, F. Structure prediction of protein-ligand complexes from sequence information with umol. *Nature Communications* **15**, 4536 (2024).
- [7] Abramson, J. *et al.* Accurate structure prediction of biomolecular interactions with alphafold 3. *Nature* 1–3 (2024).
- [8] Stärk, H., Ganea, O., Pattanaik, L., Barzilay, R. & Jaakkola, T. Equibind: Geometric deep learning for drug binding structure prediction. In *International conference on machine learning*, 20503–20521 (PMLR, 2022).
- [9] Lu, W. *et al.* Tankbind: Trigonometry-aware neural networks for drug-protein binding structure prediction. *Advances in neural information processing systems* **35**, 7236–7249 (2022).
- [10] Zhang, Y., Cai, H., Shi, C., Zhong, B. & Tang, J. E3bind: An end-to-end equivariant network for protein-ligand docking. *arXiv preprint arXiv:2210.06069* (2022).
- [11] Krivák, R. & Hoksza, D. P2rank: machine learning based tool for rapid and accurate prediction of ligand binding sites from protein structure. *Journal of Cheminformatics* **10**, 39 (2018).
- [12] Jumper, J. *et al.* Highly accurate protein structure prediction with alphafold. *Nature* **596**, 583–589 (2021).
- [13] Pei, Q. *et al.* Fabind: Fast and accurate protein-ligand binding. *Advances in Neural Information Processing Systems* **36** (2024).
- [14] Corso, G., Stärk, H., Jing, B., Barzilay, R. & Jaakkola, T. Diffdock: Diffusion steps, twists, and turns for molecular docking. *arXiv preprint arXiv:2210.01776* (2022).
- [15] Lin, Z. *et al.* Language models of protein sequences at the scale of evolution enable accurate structure prediction. *BioRxiv* **2022**, 500902 (2022).
- [16] Landrum, G. *et al.* Rdkit: Open-source cheminformatics. URL <https://www.rdkit.org>.
- [17] Liu, Z. *et al.* Forging the basis for developing protein–ligand interaction scoring functions. *Accounts of Chemical Research* **50**, 302–309 (2017).
- [18] Buttenschoen, M., Morris, G. M. & Deane, C. M. Posebusters: Ai-based docking methods fail to generate physically valid poses or generalise to novel sequences. *Chemical Science* **15**, 3130–3139 (2024).
- [19] Alhossary, A., Handoko, S. D., Mu, Y. & Kwoh, C.-K. Fast, accurate, and reliable molecular docking with quickvina 2. *Bioinformatics* **31**, 2214–2216 (2015).
- [20] Hassan, N. M., Alhossary, A. A., Mu, Y. & Kwoh, C.-K. Protein-ligand blind docking using quickvina-w with inter-process spatio-temporal integration. *Scientific Reports* **7**, 15451 (2017).
- [21] McNutt, A. T. *et al.* Gnina 1.0: molecular docking with deep learning. *Journal of Cheminformatics* **13**, 43 (2021).
- [22] Meli, R. & Biggin, P. C. spyrmsd: symmetry-corrected rmsd calculations in python. *Journal of Cheminformatics* **12**, 49 (2020).
- [23] Floristean, C., Bouatta, N. & AlQuraishi, M. *Unpublished Work* .
- [24] Kabsch, W. A solution for the best rotation to relate two sets of vectors. *Acta Crystallographica Section A: Crystal Physics, Diffraction, Theoretical and General Crystallography* **32**, 922–923 (1976).

- [25] Lyu, J. *et al.* Ultra-large library docking for discovering new chemotypes. *Nature* **566**, 224–229 (2019).
- [26] Moriwaki, H., Tian, Y.-S., Kawashita, N. & Takagi, T. Mordred: a molecular descriptor calculator. *Journal of Cheminformatics* **10**, 4 (2018).
- [27] Kitazume, S. *et al.* Alzheimer’s  $\beta$ -secretase,  $\beta$ -site amyloid precursor protein-cleaving enzyme, is responsible for cleavage secretion of a golgi-resident sialyltransferase. *Proceedings of the National Academy of Sciences* **98**, 13554–13559 (2001).
- [28] Li, S., Pritchard, D. M. & Yu, L.-G. Galectin-3 promotes secretion of proteases that decrease epithelium integrity in human colon cancer cells. *Cell Death & Disease* **14**, 268 (2023).
- [29] Gilson, M. K. *et al.* Bindingdb in 2015: a public database for medicinal chemistry, computational chemistry and systems pharmacology. *Nucleic acids research* **44**, D1045–D1053 (2016).
- [30] Lu, W. *et al.* Dynamicbind: predicting ligand-specific protein-ligand complex structure with a deep equivariant generative model. *Nature Communications* **15**, 1071 (2024).
- [31] Nakata, S., Mori, Y. & Tanaka, S. End-to-end protein–ligand complex structure generation with diffusion-based generative models. *BMC Bioinformatics* **24**, 233 (2023).
- [32] Evans, R. *et al.* Protein complex prediction with alphafold-multimer. *bioRxiv* 2021–10 (2021).
- [33] Paszke, A. *et al.* Pytorch: An imperative style, high-performance deep learning library. *Advances in neural information processing systems* **32** (2019).
- [34] Falcon, W. & The PyTorch Lightning team. PyTorch Lightning (2019). URL <https://github.com/Lightning-AI/lightning>.
- [35] Ahdriz, G. *et al.* Openfold: Retraining alphafold2 yields new insights into its learning mechanisms and capacity for generalization. *Nature Methods* 1–11 (2024).
- [36] Loshchilov, I. & Hutter, F. Decoupled weight decay regularization. *arXiv preprint arXiv:1711.05101* (2017).
- [37] Kingma, D. P. & Ba, J. Adam: A method for stochastic optimization. *arXiv preprint arXiv:1412.6980* (2014).
- [38] Nguyen, H., Case, D. A. & Rose, A. S. Nglview–interactive molecular graphics for jupyter notebooks. *Bioinformatics* **34**, 1241–1242 (2018).
- [39] Chen, L. *et al.* TransformerCPI: improving compound–protein interaction prediction by sequence-based deep learning with self-attention mechanism and label reversal experiments. *Bioinformatics* **36**, 4406–4414 (2020).
- [40] Li, S. *et al.* Monn: a multi-objective neural network for predicting compound-protein interactions and affinities. *Cell Systems* **10**, 308–322 (2020).
- [41] Moon, S., Zhong, W., Yang, S., Lim, J. & Kim, W. Y. Pignet: a physics-informed deep learning model toward generalized drug–target interaction predictions. *Chemical Science* **13**, 3661–3673 (2022).
- [42] Jiang, D. *et al.* InteractionGraphNet: A novel and efficient deep graph representation learning framework for accurate protein–ligand interaction predictions. *Journal of Medicinal Chemistry* **64**, 18209–18232 (2021).
- [43] Somnath, V. R., Bunne, C. & Krause, A. Multi-scale representation learning on proteins. *Advances in Neural Information Processing Systems* **34**, 25244–25255 (2021).
- [44] Wang, P. *et al.* Structure-aware multimodal deep learning for drug–protein interaction prediction. *Journal of Chemical Information and Modeling* **62**, 1308–1317 (2022).
- [45] Rogers, D. & Hahn, M. Extended-connectivity fingerprints. *Journal of Chemical Information and Modeling* **50**, 742–754 (2010).

## Supplementary Information

### SI.1 Algorithms

**Algorithm 1** QUICKBIND architecture. Module names correspond to the names of the algorithms in the supplementary information of [12] and the same notation is used. The Evoformer Stack does not contain the MSAColumnAttention module. New modules are highlighted in blue. Concatenation (concat) and deconcatenation (deconcat) happens along the sequence and atom dimension, unless otherwise stated.  $\{r_i\}$ , protein features.  $\{l_i\}$ , ligand features.  $\{\vec{x}_{C_\alpha}\}$ ,  $\{\vec{x}_C\}$ ,  $\{\vec{x}_N\}$ , coordinates of  $C_\alpha$ , C, and N atoms.  $\{\vec{t}_i^{\text{lig}}\}$ , initial ligand coordinates.  $\{f_i^{\text{res\_index}}\}$ , indices of amino acid residues.  $\{f_{ij}^{\text{adj}}\}$ , ligand adjacency matrix.

---

```

1: function QUICKBIND( $\{r_i\}$ ,  $\{l_i\}$ ,  $\{\vec{x}_{C_\alpha}\}$ ,  $\{\vec{x}_C\}$ ,  $\{\vec{x}_N\}$ ,  $\{\vec{t}_i^{\text{lig}}\}$ ,  $\{f_i^{\text{res\_index}}\}$ ,  $\{f_{ij}^{\text{adj}}\}$ )
2:    $\{\vec{X}_C^{\text{pseudo}}\}$ ,  $\{\vec{X}_N^{\text{pseudo}}\} \leftarrow \text{getadjacentatoms} \left( \{\vec{t}_i^{\text{lig}}\} \right)$  # as described in Methods
3:    $T_i^{\text{lig}} \leftarrow \text{rigidFrom3Points} \left( \vec{t}_i^{\text{lig}}, \vec{x}_C^{\text{pseudo}}, \vec{x}_N^{\text{pseudo}} \right)$ 
4:    $T_i^{\text{prot}} \leftarrow \text{rigidFrom3Points} \left( \vec{x}_{C_\alpha}, \vec{x}_C, \vec{x}_N \right)$ 
5:    $\{T_i\} \leftarrow \text{concat} \left( \{T_i^{\text{prot}}\}, \{T_i^{\text{lig}}\} \right)$ 
6:    $\{s_i\}$ ,  $\{z_{ij}\} \leftarrow \text{InputEmbedder} \left( \{r_i\}, \{l_i\}, \{\vec{x}_{C_\alpha}\}, \{\vec{t}_i^{\text{lig}}\}, \{f_i^{\text{res\_index}}\}, \{f_{ij}^{\text{adj}}\} \right)$ 
7:   # Evoformer
8:    $\{s_i\}$ ,  $\{z_{ij}\} \leftarrow \text{EvoformerStack} (\{s_i\}, \{z_{ij}\})$ 
9:   # Structure Module
10:   $s_i \leftarrow \text{LayerNorm} (s_i)$ 
11:   $z_{ij} \leftarrow \text{LayerNorm} (z_{ij})$ 
12:   $s_i \leftarrow \text{Linear} (s_i)$ 
13:  for all  $l \in [1, \dots, N_{\text{Struct}}]$  do
14:     $\{s_i\} += \text{InvariantPointAttention} (\{s_i\}, \{z_{ij}\}, \{T_i\})$ 
15:     $s_i \leftarrow \text{LayerNorm} (\text{Dropout}_{0.1} (s_i))$ 
16:     $s_i \leftarrow s_i + \text{Linear} (\text{relu} (\text{Linear} (\text{relu} (\text{Linear} (s_i))))))$ 
17:     $s_i \leftarrow \text{LayerNorm} (\text{Dropout}_{0.1} (s_i))$ 
18:     $\{T_i^{\text{prot}}\}, \{T_i^{\text{lig}}\} \leftarrow \text{deconcat} (\{T_i\})$ 
19:     $T_i^{\text{lig}} \leftarrow T_i^{\text{lig}} \circ \text{BackboneUpdate} (s_i)$  # Use predicted quaternion and
20:     $\{T_i\} \leftarrow \text{concat} \left( \{T_i^{\text{prot}}\}, \{T_i^{\text{lig}}\} \right)$  # translation to update ligand frames
21:  end for
22:   $\{\mathbf{R}_i^{\text{lig}}\}, \{\vec{t}_i^{\text{lig}}\} = \{T_i^{\text{lig}}\}$ 
23:  return  $\{\vec{t}_i^{\text{lig}}\}$ 
24: end function

```

---

---

**Algorithm 2** Algorithm for the generation of input embeddings.

---

```
1: function INPUTEMBEDDER( $\{r_i\}$ ,  $\{l_i\}$ ,  $\{\vec{x}_{C_\alpha}\}$ ,  $\{\vec{t}_i^{\text{lig}}\}$ ,  $\{f_i^{\text{res\_index}}\}$ ,  $\{f_{ij}^{\text{adj}}\}$ )
2:    $r_i \leftarrow \text{Linear}(r_i)$ 
3:    $l_i \leftarrow \text{Linear}(l_i)$ 
4:    $\{s_i\} \leftarrow \text{concat}(\{r_i\}, \{l_i\})$ 
5:    $a_i \leftarrow \text{Linear}(s_i)$ 
6:    $b_i \leftarrow \text{Linear}(s_i)$ 
7:    $z_{ij} \leftarrow a_i + b_j$ 
8:    $\{p_{ij}\} \leftarrow \text{relpos}(\{f_i^{\text{res\_index}}\})$ 
9:    $q_{ij} \leftarrow \text{Linear}(f_{ij}^{\text{adj}})$ 
10:   $\{\omega_{ij}\} \leftarrow \text{blockdiag}(\{p_{ij}\}, \{q_{ij}\})$  # combine into a blockdiagonal tensor
11:   $d_{ij}^{\text{prot}} \leftarrow \text{Linear}\left(\left\|\vec{x}_{C_\alpha}^i - \vec{x}_{C_\alpha}^j\right\|_2\right)$ 
12:   $d_{ij}^{\text{lig}} \leftarrow \text{Linear}\left(\left\|\vec{t}_i^{\text{lig}} - \vec{t}_j^{\text{lig}}\right\|_2\right)$ 
13:   $\{d_{ij}\} \leftarrow \text{blockdiag}(\{d_{ij}^{\text{prot}}\}, \{d_{ij}^{\text{lig}}\})$  # combine into a blockdiagonal tensor
14:   $z_{ij} = z_{ij} + \omega_{ij} + d_{ij}$ 
15:   $s_i \leftarrow \text{Linear}(s_i)$ 
16:  return  $\{s_i\}$ ,  $\{z_{ij}\}$ 
17: end function
```

---

---

**Algorithm 3** Algorithm for updating the ligand frames.

---

```
1: function BACKBONEUPDATE( $\{s_i\}$ )
2:    $\{s_i^{\text{prot}}\}, \{s_i^{\text{lig}}\} \leftarrow \text{deconcat}(\{s_i\})$ 
3:    $m_i \leftarrow \text{MultiHeadAttention}(q = \{s_i^{\text{lig}}\}, k = \{s_i^{\text{prot}}\}, v = \{s_i^{\text{prot}}\})$ 
4:    $s_i^{\text{lig}} += m_i$ 
5:    $b_i, c_i, d_i, \vec{t}_i \leftarrow \text{Linear}(s_i^{\text{lig}})$  # quaternion and translation
6:   return  $b_i, c_i, d_i, \vec{t}_i$ 
7: end function
```

---

---

**Algorithm 4** Algorithm for getting the coordinates of a dummy atom when an atom has only one neighbor. Find the vector with the same  $x$  and  $y$  coordinates as the bond vector between the atom under question and its one neighbor, such that the dot product of the two vanishes, and subtract that vector from the coordinates of the given atom.  $\vec{x}_C$ , coordinates of atom under consideration,  $\vec{x}_N$ , coordinates of its neighbor.

---

```
1: function GETDUMMYATOMCOORDS( $\vec{x}_C, \vec{x}_N$ )
2:    $\vec{b} \leftarrow \vec{x}_C - \vec{x}_N$ 
3:    $x_b, y_b, z_b \leftarrow \vec{b}$  # get  $x, y, z$  coordinates
4:    $z'_b \leftarrow -\frac{x_b^2 + y_b^2}{z_b}$ 
5:    $\vec{b}' \leftarrow \begin{pmatrix} x_b \\ y_b \\ z'_b \end{pmatrix}$  #  $\vec{b} \cdot \vec{b}' = 0$ 
6:    $\vec{x}_{N'} \leftarrow \vec{x}_C - \vec{b}'$ 
7:   return  $\vec{x}_{N'}$ 
8: end function
```

---

---

**Algorithm 5** Binding affinity prediction model.

---

```
1: function BINDINGAFFINITYPREDICTOR( $\{s_i\}$ )
2:    $s_i \leftarrow \text{LayerNorm}(s_i)$ 
3:    $s_i \leftarrow \text{Linear}(\text{silu}(\text{Linear}(s_i)))$ 
4:    $a \leftarrow \text{mean}(\{s_i\})$  # along sequence dimension
5:    $a \leftarrow \text{Linear}(\text{relu}(\text{Linear}(\text{relu}(\text{Linear}(a))))))$  #  $\mathbb{R}^{64} \rightarrow \mathbb{R}^{32} \rightarrow \mathbb{R}$ 
6:   return  $a$ 
7: end function
```

---

## SI.2 Protein and ligand features

Residue types are one-hot encoded. Ligand atoms have the following features: atomic number (H, C, N, O, F, P, S, Cl, Br, I, other), chirality, degree (1 through 4, or other), formal charge (-1, 0, 1, or other), number of connected H atoms (0 through 3, or other), hybridization, presence in a ring, and presence in an aromatic ring. Early versions included atomic numbers 1 through 119, degrees up to 10, formal charges of -5 through 5, implicit valence, number of connected hydrogens of up to 8, number of radical electrons, hybridization, presence in an aromatic ring, the number of rings it is in, presence in a ring of size 3, 4, 5, 6, 7, or 8, similar to ref. [8]. These additional features did not improve performance and so were omitted. Ligand coordinates are initialized using a random RDKit conformer [16].

## SI.3 Cropping

To reduce QUICKBIND’s memory footprint during training, input protein sequences were cropped to 512 or 256 residues for models without and with the Evoformer module, respectively. Since model performance drops noticeably for shorter crop sizes, the final model was finetuned with a crop size of 512 residues. At inference time, the full protein sequence is used. Depending on available GPU memory, inference might therefore have to be run on CPUs. Using our resources, we had to restrict inference on GPUs to proteins shorter than 2,000 residues. For multi-chain proteins, sequences were concatenated in the order in which they appear in the PDB file.

We tested different cropping strategies: random contiguous cropping; setting the residue whose  $C_\alpha$  atom is closest to any ligand atom as the midpoint of the contiguous cropped fragment (binding site cropping, BSC); selecting the  $x$  residues closest to any ligand atom (spatial cropping), and a setting in which the protein was cropped randomly or spatially with a probability of 0.5.

## SI.4 Hyperparameter screening

Because extensive hyperparameter screening of the full QUICKBIND model would have been too computationally expensive, we optimized many hyperparameters and architectural choices using two smaller variants, both trained without ligand frames and still updating H atom positions:

- QUICKBIND-S, which lacks the Evoformer module and contains just four or eight Structure module blocks with unshared weights, trained without batching.
- QUICKBIND-M, which lacks Triangle Attention in the Evoformer stack (its most expensive module), trained with a batch size of 12 or 16.

The main results of the hyperparameter screening are summarized in Table SI.1. Furthermore, several ways to generate the ligand coordinate updates from the final single representation were tested. In general, the final single representation is separated into a protein and a ligand single representation. Then, either:

- only the ligand single representation is passed through a linear layer to produce the coordinate updates, or
- the protein single representation is summed along the sequence dimension or the corresponding mean is taken, and this pooled protein representation is concatenated with the ligand single representation before passing it through the linear layer, or

- the outer product of the protein and ligand single representations is summed along the sequence dimension or the corresponding mean is taken, and then passed through the linear layer, or
- the output of an attention layer with the query vectors coming from the ligand and key and value vectors coming from the protein are concatenated with the ligand single representation and passed through the final linear layer.

The last approach led to the best results.

We also tested scaling the coordinate update by a factor of 10, as is done in AF2, but did not find this to improve model performance. Furthermore, we briefly experimented with first applying a global roto-translation of the ligand coordinates, and then either finetuning all ligand coordinates or just changing the torsion angles of rotatable bonds, but did not find this to lead to better results. Using a gated variant of the IPA module [23] improved model performance compared to the standard IPA module. In addition, we also tested two ideas from ALPHAFOLD-MULTIMER (AF-MULTIMER) [32], moving the outer product mean to the beginning of the Evoformer block and the multimer version of the relative positional encoding, but neither improved model performance.

## SI.5 Training details

QUICKBIND was implemented using PyTorch [33], PyTorch Lightning [34], OpenFold [35], and the RDKit [16]. Models were trained using the AdamW optimizer [36] with a learning rate and a weight decay coefficient of  $10^{-4}$ , early stopping with a patience of 50 epochs, and a batch size of 16. The binding affinity prediction model was trained using the Adam optimizer [37] with a learning rate of 0.01, early stopping with a patience of 50 epochs, and a batch size of 64 using a mean squared error (MSE) loss. The model weights with the best performance on the validation set were chosen for evaluation on the test set. Training the final QUICKBIND model took several weeks on eight NVIDIA A40 GPUs, but QUICKBIND-S and QUICKBIND-M variants were trained in two weeks or less. The final model was trained with 5 different seeds. Some replicas got stuck in local minima (success rates of 0.0%, 2.5%, 12.1%, 15.4%, 23.4%), and only the best-performing model was finetuned with a crop size of 512. It is plausible that models that got stuck in local minima would have reached a similar performance to the final model after the finetuning stage, but we did not test this because the training time when including triangle attention scales very unfavorably with sequence length. Force-field minimization was performed as described in ref. [18] using a script kindly provided by one of the authors. Visualizations were generated using NGLview [38].



Table SI.1: Results of hyperparameter search. Accepted configurations are indicated by ✓ or underlined, rejected configurations are indicated by ✗.  $\mathcal{L}_{\text{MSE}}$  - Mean squared error loss.  $\mathcal{L}_{\text{centroid}}$  - Centroid loss.  $\mathcal{L}_{\text{Kabsch}}$  - Kabsch loss.  $\mathcal{L}_{\text{FAPE}}$  - FAPE loss.  $\mathcal{L}_{\text{FAPE}}$  was tested with a  $\mathcal{L}_{\text{FAPE}}^{\text{prot-lig}}$  clamped at 10 Å and without clamping.  $\mathcal{L}_{\text{FAPE}}^{\text{aux}}$  - intermediate FAPE losses acting on the outputs of every Structure module block.  $\mathcal{L}_{\text{dist}}^{\text{lig-lig}}$  - ligand distogram loss head, a cross-entropy loss that acts on a symmetrized version of the ligand pair representation, similar to AF2, with 42 distance bins between 1 and 5 Å.  $\mathcal{L}_{\text{dist}}^{\text{prot-lig}}$  - protein-ligand distogram loss head using the symmetrized off-diagonal parts of the pair representation, using the same bins as in AF2.  $\mathcal{L}_{\text{torsion}}$  - torsion angle loss. Black hole initialization refers to collapsing all ligand atoms at the origin, as is done in AF2.

<b>Input embeddings</b>	
Pairwise distances	✓
Radial basis projection of pairwise distances	✗
AF2 relative positional encoding	✓
AF2-MULTIMER relative positional encoding	✗
Adjacency matrix	✓
... w/ one-hot encoded bond types	✗
... w/ topological distance	✗
<b>Loss function</b>	
$\mathcal{L}_{\text{MSE}}, \mathcal{L}_{\text{centroid}}, \mathcal{L}_{\text{Kabsch}}, \mathcal{L}_{\text{FAPE}}$ (clamped and <u>unclamped</u> ) , $\mathcal{L}_{\text{FAPE}}^{\text{aux}}, \mathcal{L}_{\text{dist}}^{\text{lig-lig}}, \mathcal{L}_{\text{dist}}^{\text{prot-lig}}, \mathcal{L}_{\text{torsion}}$	
<b>Cropping</b>	
Random	✗
Binding site cropping	✓
Spatial cropping	✗
Random and spatial cropping	✗
<b>Ligand frames</b>	
Keeping the rotation matrix fixed	✗
Updating the rotation matrix	✓
<b>Ligand initialisation</b>	
At origin	✓
Black hole initialisation	✗
Randomly translated and rotated	✗
<b>Structure module</b>	
Number of blocks	4, <u>8</u>
<b>Evoformer</b>	
Number of blocks	8, <u>12</u>
Number of MSA attention heads	<u>8</u> , 12

## SI.6 Exemplary predictions

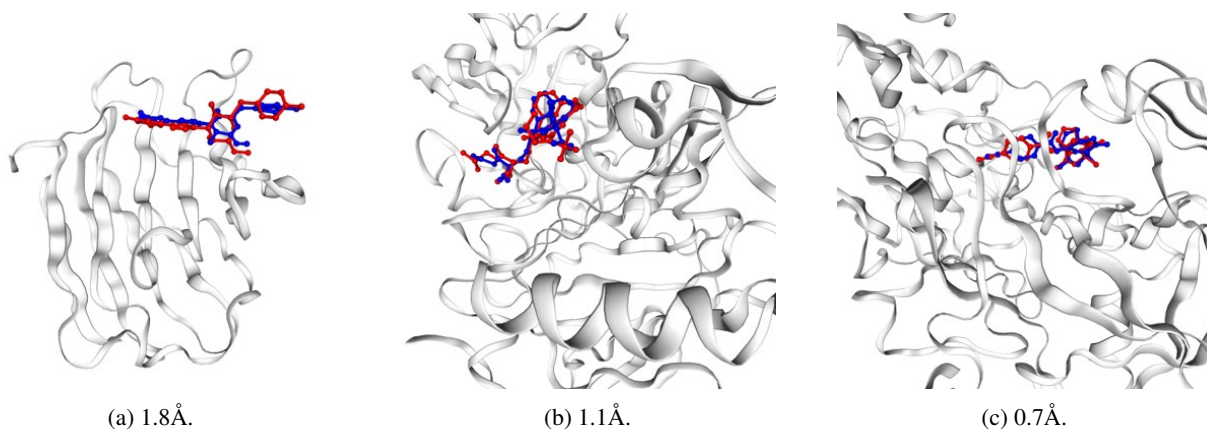


Figure SI.1: Three examples of QUICKBIND predictions and their RMSDs, randomly chosen from 100 lowest-RMSD predictions on the PDBBind test set. The ground-truth ligand is shown in red, the QUICKBIND prediction is shown in blue.

## SI.7 PB failure modes

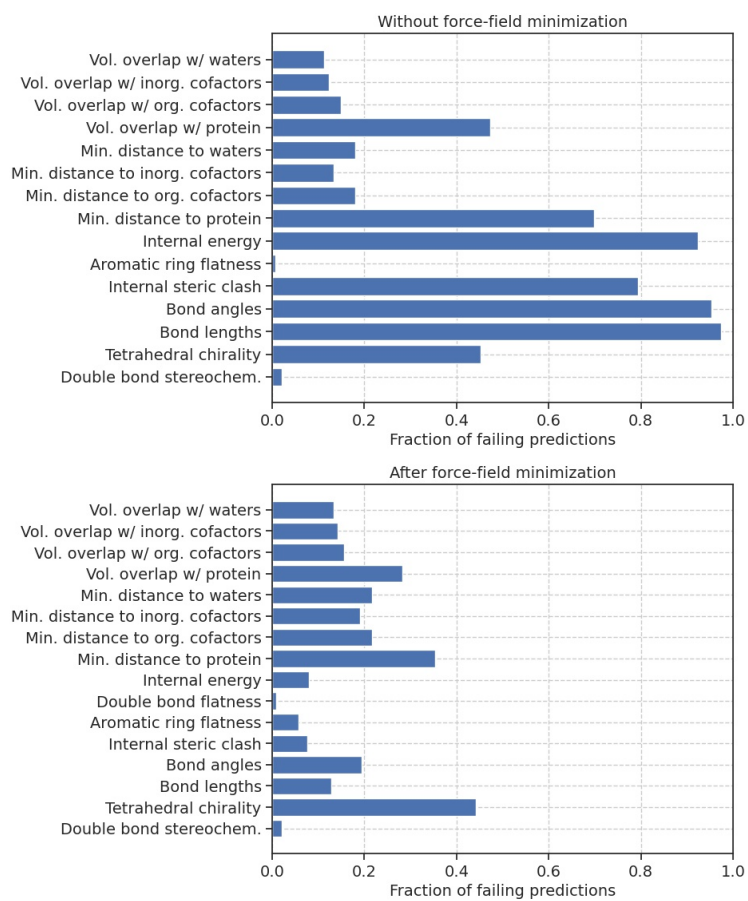


Figure SI.2: Fraction of all QUICKBIND predictions on the PB test set that fail PB tests, before and after force field minimization.

## SI.8 Correlation with physicochemical features

Table SI.2: Correlation between physicochemical features of the ligand and mean channel values of the molecule representation. The magnitude of the Pearson's  $R$  values for the octanol-water partition coefficient and number of aromatic rings was less than 0.6.

Feature	Pearson's $R$	$p$ -value	Channel
Total hydrophobic surface area	-0.72	$10^{-59}$	57
Molecular weight	0.73	$10^{-62}$	27
Number of hydrogen bond acceptors	0.63	$10^{-42}$	11
Number of hydrogen bond donors	0.70	$10^{-54}$	31
Polar surface area	0.71	$10^{-56}$	27
Number of rotatable bonds	0.76	$10^{-70}$	27

## SI.9 Additional interpretability studies

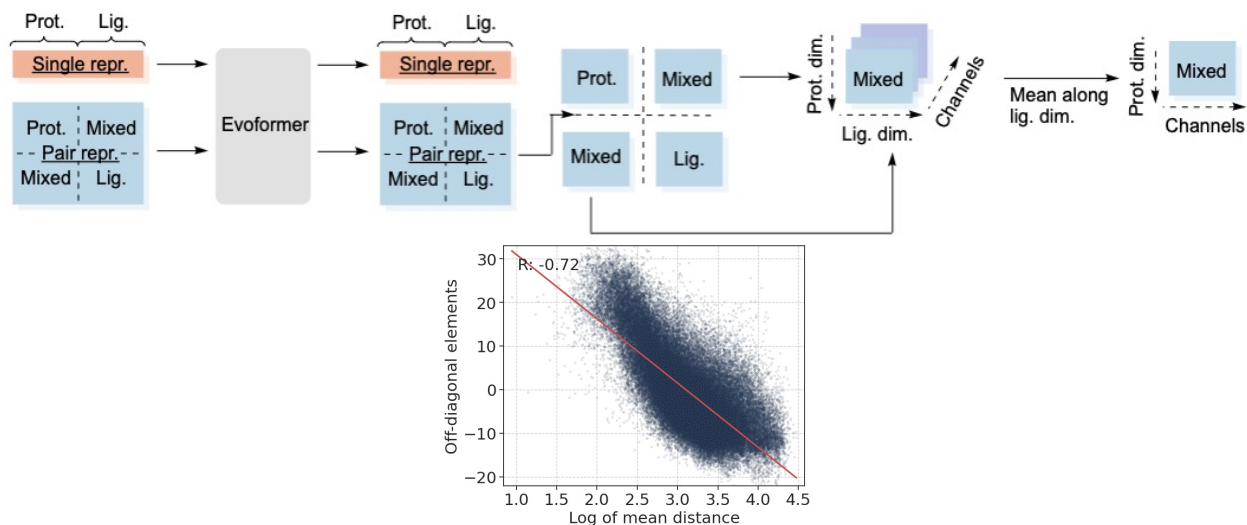


Figure SI.3: The off-diagonal elements of the pair representation contain information about the final ligand atom positions relative to the protein. The off-diagonal elements of the pair representation after the Evoformer block were symmetrized and the mean along the ligand dimension was taken. Some channel values correlate with the logarithm of the mean  $C_{\alpha}$ -ligand atom distance; for one particular channel the Pearson's R value is -0.72 at a  $p$ -value smaller than machine precision.

We wanted to understand how QUICKBIND obtains its initial guess of the docked ligand pose. The pair representation contains a protein and a ligand block, as well as mixed off-diagonal elements. Among other features, the protein and ligand blocks are constructed from the pairwise distances of the  $C_{\alpha}$  and ligand atoms, respectively, but the off-diagonal elements do not contain any spatial information. We hypothesized that the model would use these off-diagonal elements for information about the interaction of the protein and the ligand, including an initial guess about their pairwise distances. We therefore took the off-diagonal elements of the pair representation after the Evoformer block, symmetrized them by transposing the lower off-diagonal block and computing the element-wise mean, and finally took the mean along the ligand dimension to obtain an  $N_{C_{\alpha}} \times c$  dimensional matrix, where  $N_{C_{\alpha}}$  is the number of  $C_{\alpha}$  atoms and  $c$  is the hidden channel dimension (Figure SI.3). Indeed, we found that already the mean along the channel dimension is weakly correlated with the logarithm of the mean  $C_{\alpha}$ -ligand atom distance with a Pearson's R value of -0.53. This correlation is much stronger for some channels. In particular, there is a channel that correlates with the logarithm of the mean  $C_{\alpha}$ -ligand atom distance with a Pearson's R value of -0.72.

## SI.10 Binding affinity prediction

Table SI.3: Root-mean-square error (RMSE), Pearson correlation coefficient (PCC), Spearman’s rank correlation coefficient (SRCC), and mean absolute error (MAE) of QUICKBIND and other methods for binding affinity prediction on the PDDBind test set, computed using the mean and standard deviation across three runs. All methods predict negative log-transformed binding affinities. Values for other methods are taken from ref. [9].

Method	RMSE ↓	PCC ↑	SRCC ↑	MAE ↓
TransformerCPI [39]	$1.741 \pm 0.058$	$0.576 \pm 0.022$	$0.540 \pm 0.016$	$1.404 \pm 0.040$
MONN [40]	$1.438 \pm 0.027$	$0.624 \pm 0.037$	$0.589 \pm 0.011$	$1.143 \pm 0.052$
PIGNet [41]	2.64	0.51	0.49	2.1
IGN [42]	$1.433 \pm 0.028$	$0.698 \pm 0.007$	$0.641 \pm 0.014$	$1.169 \pm 0.036$
HOLOPROT [43]	$1.546 \pm 0.065$	$0.602 \pm 0.006$	$0.571 \pm 0.018$	$1.208 \pm 0.038$
STAMPDPI [44]	1.658	0.545	0.411	1.325
TANKBind [9]	$1.346 \pm 0.007$	$0.726 \pm 0.007$	$0.703 \pm 0.017$	$1.070 \pm 0.019$
QuickBind	$1.577 \pm 0.011$	$0.548 \pm 0.025$	$0.482 \pm 0.024$	$1.292 \pm 0.008$



## SI.11 Virtual screening results

Table SI.4 summarizes important characteristics of the five proteins in the PDBBind test set with the highest number of complex structures in the PDBBind test set, as well as QUICKBIND’s cross-docking performance. In particular, it contains:

- the number of complex structures in the PDBBind test set (# Binders),
- the number of complex structures in the PDBBind train set (# Train ex.),
- the average  $C_\alpha$  RMSD between input and true protein structures (BB RMSD),
- and the average Tanimoto similarity between the lowest, second-lowest, or third-lowest affinity binder and the remaining binders, calculated using extended-connectivity fingerprints [45] with a radius of 3 (TS).

We evaluate QUICKBIND’s cross-docking performance using the fraction of predictions with a ligand RMSD below  $2\text{\AA}$  ( $\% < 2\text{\AA}$ ) and the fraction of predictions with a ligand RMSD below  $5\text{\AA}$  ( $\% < 5\text{\AA}$ ), after aligning the  $C_\alpha$  atoms of the input and the true protein structure using the Kabsch algorithm. For this alignment and for calculating BB RMSD we only consider  $C_\alpha$  atoms that were successfully extracted for both complexes. Where applicable, we provide the mean and standard deviation across the three runs with the crystal structures of the lowest, second-lowest, and third-lowest affinity binder. For all proteins, we tested if the predicted binding affinities of binders were higher than those of non-binders using one-sided Wilcoxon rank-sum tests.

Table SI.4: Characteristics of the five proteins in the PDBBind test set with the highest number of complex structures and QUICKBIND’s cross-docking performance.

UniProt ID	# Binders	# Train ex.	$\% < 2\text{\AA}$	$\% < 5\text{\AA}$	BB RMSD [ $\text{\AA}$ ]	TS
B1MDI3	19	0	$0.0 \pm 0.0$	$2 \pm 3$	$0.36 \pm 0.09$	$0.26 \pm 0.08$
P56817	16	308	$73 \pm 0$	$93 \pm 0$	$0.96 \pm 0.04$	$0.209 \pm 0.005$
P17931	15	22	$86 \pm 0$	$93 \pm 0$	$0.21 \pm 0.07$	$0.620 \pm 0.029$
Q8ULI9	14	3	$100 \pm 0$	$100 \pm 0$	$0.15 \pm 0.01$	$0.64 \pm 0.10$
P01116	13	8	$0.0 \pm 0.0$	$17 \pm 12$	$7.7 \pm 2.7$	$0.101 \pm 0.026$

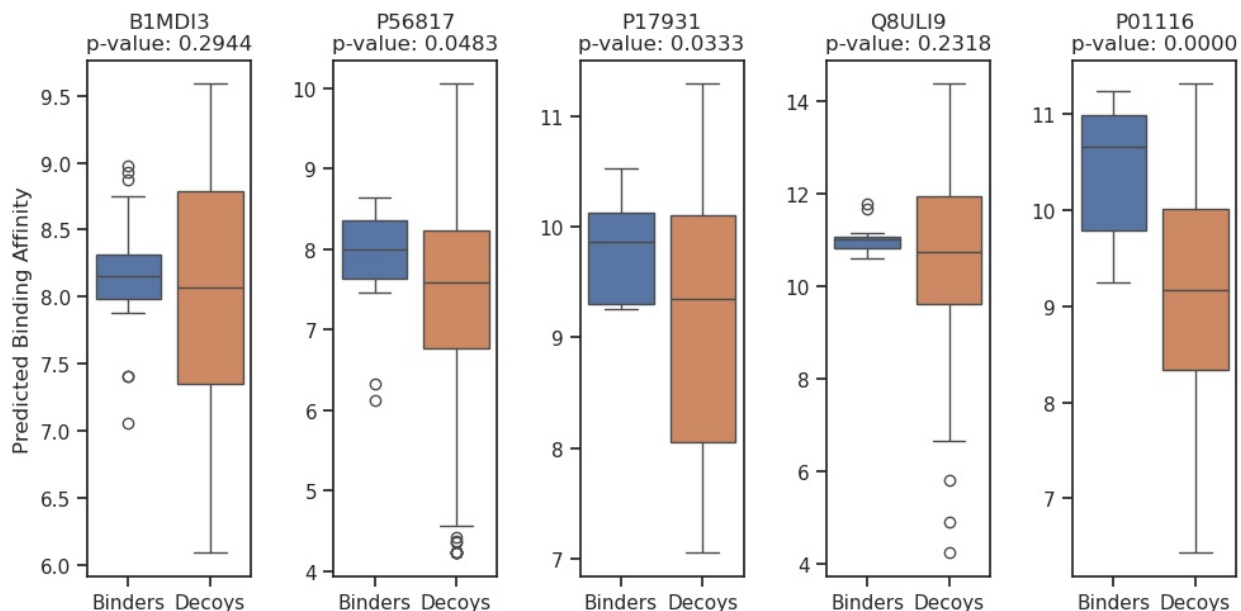


Figure SI.4: Predicted binding affinities of true binders and decoys for the five proteins in the PDBBind test set with the highest number of binders, using the protein structure of the lowest affinity binder.

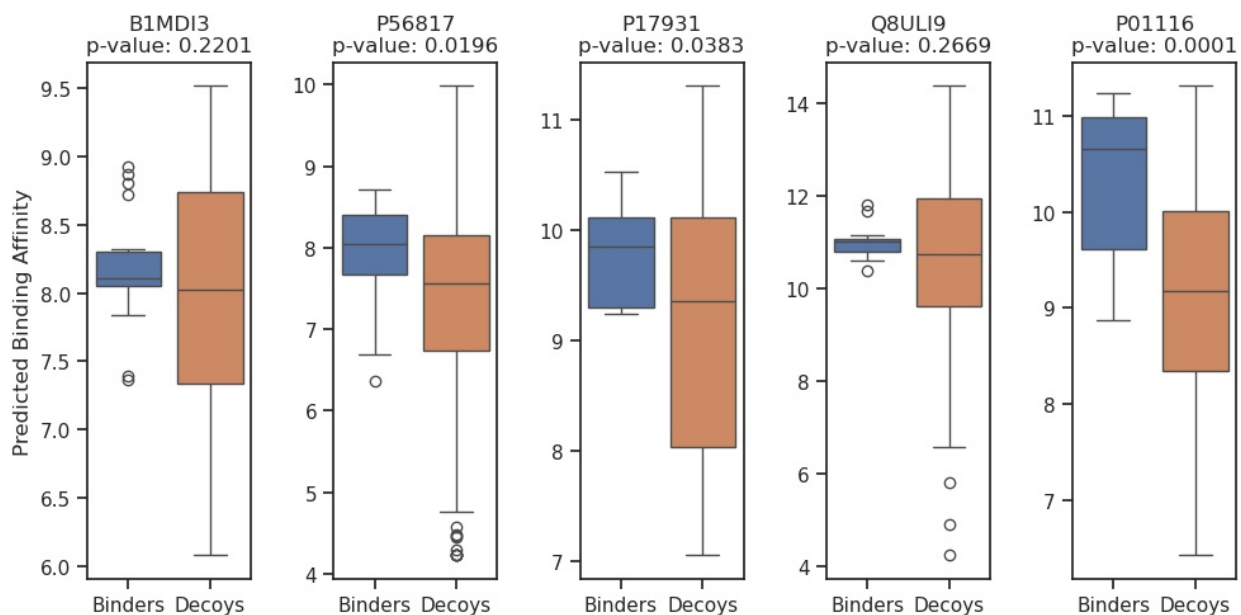


Figure SI.5: Predicted binding affinities of true binders and decoys for the five proteins in the PDBBind test set with the highest number of binders, using the protein structure of the second-lowest affinity binder.

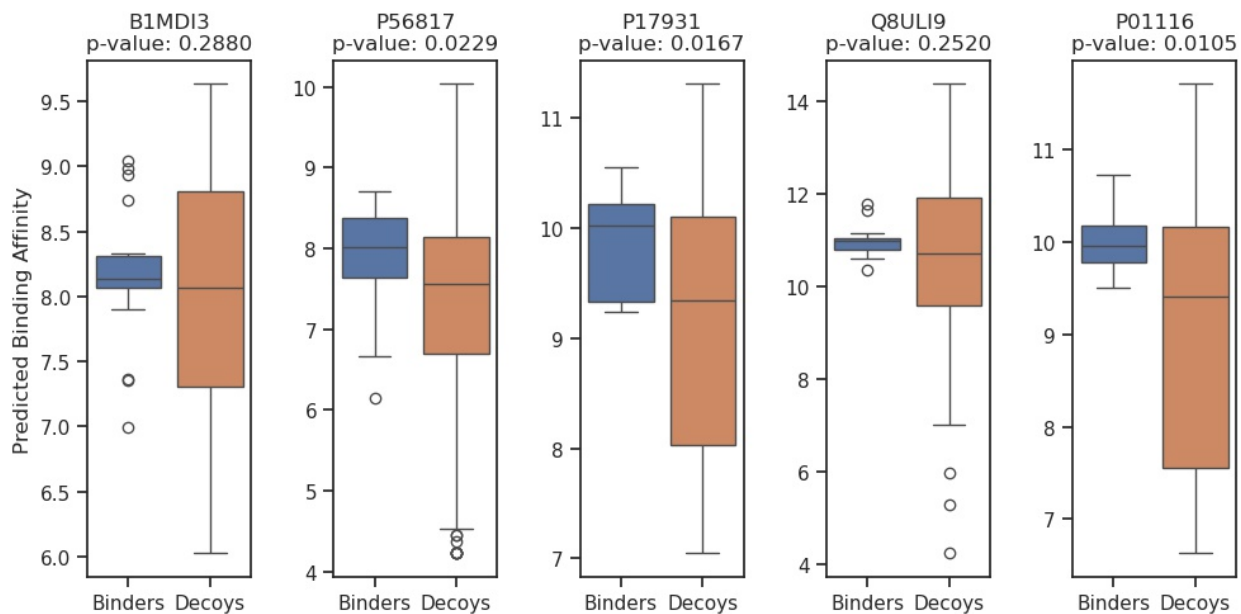


Figure SI.6: Predicted binding affinities of true binders and decoys for the five proteins in the PDBBind test set with the highest number of binders, using the protein structure of the third-lowest affinity binder.

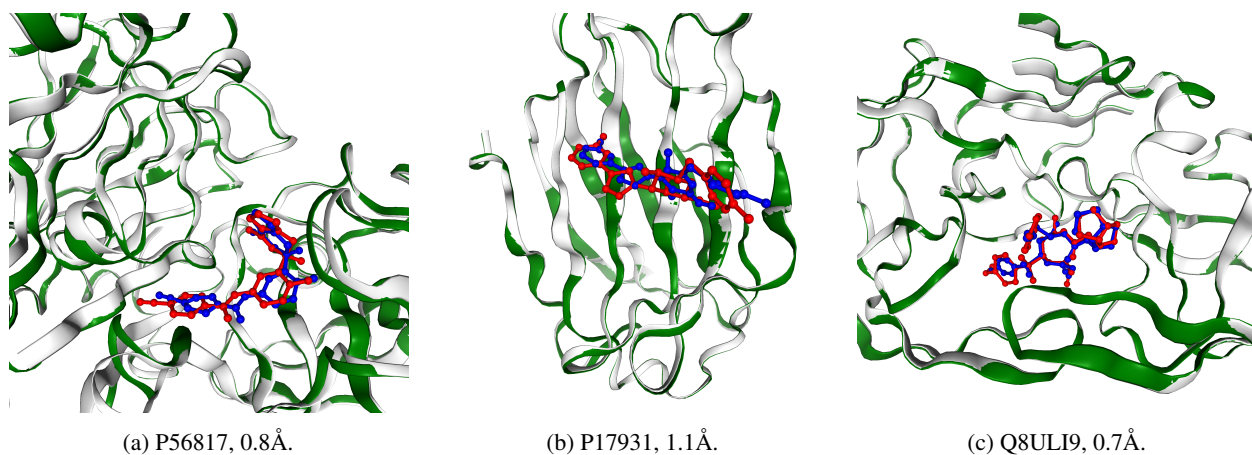


Figure SI.7: Lowest RMSD QUICKBIND cross-docking predictions for P56817, P17931, and Q8ULI9. The ground-truth ligand and protein are shown in red and white, respectively. The input protein structure is shown in green and the QUICKBIND prediction is shown in blue.

## SI.12 Retrospective comparison with AF3

In this section we discuss our observations on the differences introduced to AF2 by QUICKBIND versus those made by AF3.

First, AF3 no longer uses residue reference frames and eschews SE(3)-equivariance entirely. In early internal experiments on QUICKBIND, we similarly observed higher success rates when ligand reference frames were omitted. We opted to include them as the model would otherwise not be equivariant to the inputted global orientation of the protein-ligand complex, which is not desirable for docking applications. This decision was however driven by the fact that QUICKBIND uses an existing protein structure instead of predicting it from scratch. For a co-folding model, abandoning reference frames and SE(3)-equivariance is therefore consistent with our findings.

Second, AF3 replaces the Evoformer with the Pairformer module. QUICKBIND’s modified Evoformer is architecturally a middle ground between the two. Similar to the Pairformer, it operates only on single and pair representations without column-wise attention. In the case of QUICKBIND, our design was informed by its use of an input protein structure, which obviated the need for a multiple sequence alignment and corresponding representation. In the Pairformer, the single representation does not update the pair representation via the outer product mean (OPM) module, and the update order of the single and pair representations is swapped. In AF-MULTIMER [32], the OPM is moved to the beginning of the Evoformer. We found the original OPM position to be more optimal (see section SI.4), but did not try omitting it, or swapping the single and pair update order.

Third, AF3 uses larger crop sizes than AF2 and AF-MULTIMER. AF3 is initially trained with a crop size of 384 then finetuned in two stages with crop sizes of 640 and 768, whereas AF2 and AF-MULTIMER were trained with crop sizes of 256 and 384 then finetuned on crop sizes of 384 and 640, respectively. We initially trained QUICKBIND on 256 residue crops, then finetuned it using 512 residue crops. We found finetuning with larger crops to be important for model performance, observing consistent improvements as crop sizes increased. Given AF3’s training procedure, this suggests that QUICKBIND would benefit from additional finetuning stages with incrementally larger crops.

Fourth, AF3 randomly chooses from contiguous, spatial, and spatial interface cropping. QUICKBIND’s cropping strategy, binding site cropping, can be considered a compromise between AF3’s two spatial cropping strategies and contiguous cropping. We tested spatial and contiguous cropping but found that binding site cropping leads to better results. Unlike QUICKBIND, AF3 cropping is applied to all tokens such that the model may only see parts of the ligand, while in QUICKBIND only the protein is cropped.

Fifth, AF3 contains a distogram head similar to the one in AF2, including a minimum distance bin of 2Å which is overly large for small molecules (C-C bonds are 1.54Å long). This suggests it primarily benefits overall complex prediction and rough positioning of ligand atoms, consistent with our observation that a distogram head does not improve QUICKBIND’s performance.

Finally, in agreement with the fact that we found better results when not distinguishing different bond types in the ligand adjacency matrix, AF3’s bond features are binary.